MATERIALS SCIENCE

# Targeted exosome coating gene-chem nanocomplex as "nanoscavenger" for clearing α-synuclein and immune activation of Parkinson's disease

**Linying Liu[1,2,3]*, Yan Li[1,2]*, Huan Peng[1,2], Ruiyuan Liu[1,2], Weihong Ji[1,2], Zhuyan Shi[1,2], Jie Shen[1,2], Guanghui Ma[1], Xin Zhang[1,2]†**



**The most critical problem in the treatment of neurodegenerative diseases is brain neuronal protection, which can be overcome by clearing pathological substances and regulating the immune environment. In the above treatment strategies, the traditional poor drug delivery problem is inevitable. Here, we show an engineering core-shell hybrid system named rabies virus glycoprotein (RVG) peptide–modified exosome (EXO) curcumin/phenylboronic acid-poly(2-(dimethylamino)ethyl acrylate) nanoparticle/small interfering RNA targeting *SNCA* (REXO-C/ANP/S). It is a nanoscavenger for clearing α-synuclein aggregates and reducing their cytotoxicity in Parkinson's disease neurons. The motor behavior of Parkinson's disease mice is substantially improved after REXO-C/ANP/S treatment. In particular, we demonstrate that REXO-C/ANP/S is also a nanoscavenger for clearing immune activation due to its natural immature dendritic cell EXO coating. Our findings show that REXO-C/ANP/S may serve as a platform for neurodegenerative diseases treatment.**

## INTRODUCTION

For neurodegenerative diseases, gene and small-molecule drugs can be used for clearing pathological substances synergistically that cause neuronal degeneration (*1*). In Parkinson's disease (PD), α-synuclein (α-syn) aggregates are considered to be the main pathological substance (*2*, *3*). Small interfering RNA (siRNA) shows potential in rare disease or disease with no good drug options but is gene related. For example, Onpattro (patisiran) has been applied as the clinical treatment of multiple sclerosis. siRNA targeting *SNCA* (siSNCA) can down-regulate α-syn protein synthesis to inhibit the formation of α-syn aggregates and could specifically down-regulate α-syn expression without targeting β- or γ-synuclein (*4*).The neuroprotective small-molecule drug curcumin has a reducing effect on the existing α-syn aggregates (*5*–*7*). Therefore, the combination of siSNCA with curcumin can synergistically reduce the cytotoxicity of α-syn aggregates on dopaminergic neurons for PD treatment. Even so, these drugs with poor bioavailability are difficult to accumulate in the action site of target neurons because of their poor absorption and rapid metabolism (*8*, *9*). In addition, brain delivery problems are mainly manifested in the fact that it is difficult for delivery systems to pass through the blood-brain barrier (BBB) and could not accurately recognize the target cell (*10*). Synthetic gene and chemical drug (gene-chem) nanocomplexes including liposomes and polymer particles have been modified with cell-penetrating peptides or cell-targeting molecules for enhanced drug delivery in brain diseases or other disease therapy (*11*). However, synthetic nanocomplexes are easily recognized as foreigners, resulting in natural immune activation, cell apoptosis, and short blood circulation time, which is unsafe and with low efficiency (*12*). In addition, when being internalized, these synthetic carriers would undergo an endosomal-lysosomal pathway, which tends to cause drug degradation and exocytosis as well as leads to inflammasome activation (*12*). Furthermore, it is necessary to control the release of drugs in the lesion area to reduce nonspecific toxicity. Therefore, to efficiently deliver gene-chem drugs to the action site of target cells for safe PD therapy, it is necessary to develop a delivery system that could overcome these delivery bottlenecks including low BBB permeation, poor neuron targeting, inefficient endocytosis into cytoplasm, and uncontrolled drug release.

To realize the above aims, we designed a targeted exosome coating gene-chem nanocomplex as an engineering "nanoscavenger" for neuronal α-syn aggregates and immune activation of PD. Exosome is a well-researched natural source carrier for siRNA and chemical drugs, with diameter of 30 to 100 nm (*4*, *13*, *14*). It has a membrane structure on whose surface the specific protein tetraspanin CD9 facilitates direct membrane fusion and helps the internal substances directly transport into the cytoplasm of the recipient cell, which avoids lysosomal trapping (*15*, *16*). To further efficiently deliver drugs through the BBB and to the dopaminergic neurons, the first process of the engineering was constructing the shell, REXO, a targeted immature dendritic cell (imDC)–derived exosome with modification of rabies virus glycoprotein (RVG) peptide with 29 amino acids, which could specifically bind to the acetylcholine receptor expressed by neuronal cells and the BBB (*17*). Because it was difficult for exosomes to load hydrophilic gene and hydrophobic small-molecule drugs simultaneously, the second process of the engineering was achieved as a product of a gene-chem coloaded core, which is a reactive oxygen species (ROS)–responsive gene-chem drug nanocomplex loading these two drugs with different characteristics (*8*, *9*). The third process of the engineering was REXO-C/ANP/S nanoscavenger preparation. REXO was coated on the nanocomplex to form a nanoscavenger. Therefore, the engineering delivery system could efficiently cross the BBB, target neurons, and release drugs in high ROS environment of diseased dopaminergic neurons. The enriched siSNCA and curcumin could have functions on α-syn protein down-regulation and α-syn aggregate inhibition synergistically.

[1]State Key Laboratory of Biochemical Engineering, Institute of Process Engineering, Chinese Academy of Sciences, Beijing 100190, P.R. China. [2]University of Chinese Academy of Sciences, Beijing 100049, P.R. China. [3]College of Bioengineering, Beijing Polytechnic, Beijing 100176, P.R. China.
*These authors contributed equally to this work.
†Corresponding author. Email: xzhang@ipe.ac.cn

Literatures indicated that neurodegenerative diseases are immune disorders (*18*, *19*). For example, PD is an adaptive immune disorder because T cells are activated by pathological substances such as α-syn peptides (*20*). In addition, studies have indicated that immune activation of PD was associated with T helper 17 ($T_H17$) functions and that differentiated $T_H17$ cells could induce the inflammatory response (*21*). In brain diseases, the factors secreted by $T_H17$ cells would induce neuron apoptosis or death and enhance central nervous system inflammation (*22*). Moreover, regulatory T ($T_{reg}$) cells could inhibit immune activation and maintain immune stability and tolerance due to interleukin-10 (IL-10) and transforming growth factor–β (TGF-β). These cytokines could promote the survival of neurons (*23*), inhibit the differentiation of $T_H17$ cells, activate macrophages and microglia, and exert anti-inflammatory effects (*24*). In addition, neuroprotection of $T_{reg}$ cells can be exerted by inhibiting the response of microglia to stimuli-nitrated α-syn (*25*). It was well known that imDC had immunosuppressive effects and played an important role in autoimmune diseases (*26*–*28*). Inspired by this, we further speculated that exosomes derived from imDC, which coat the hybrid system REXO-C/ANP/S, might have an effect on immunosuppression as imDC does (*29*). The study further confirmed that the hybrid system REXO-C/ANP/S was effective in inhibiting $T_H17$ cell immune activation and promoting immunosuppression-related $T_{reg}$ cell functions in the nervous system.

## RESULTS

### Preparation approach and characterization of REXO-C/ANP/S

The hybrid nanoparticle (NP) REXO-C/ANP/S was prepared from two parts (Fig. 1A): preparation of gene-chem core C/ANP/S and

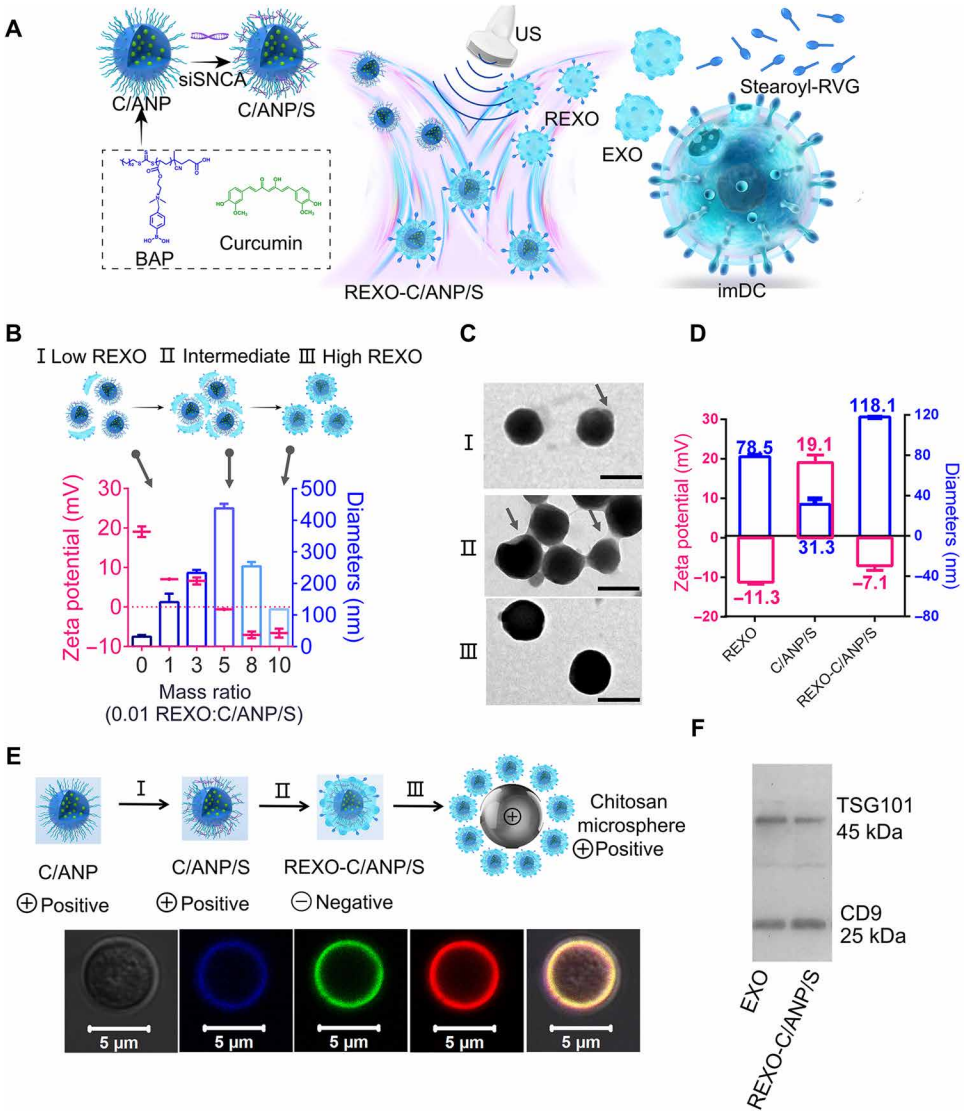


**Fig. 1. REXO-C/ANP/S preparation and characterization.** (**A**) Scheme of REXO-C/ANP/S preparation. (**B**) Zeta potential and diameters of NPs under different REXO:C/ANP/S ratios. (**C**) TEM images of NPs under different REXO:C/ANP/S ratios (I, low REXO:C/ANP/S ratio; II, intermediate; and III, high REXO:C/ANP/S ratio). Scale bars, 100 nm. (**D**) Comparison in zeta potential and diameters of REXO, C/ANP/S, and REXO/ANP/S. (**E**) Chitosan microsphere with REXO-C/ANP/S absorption. Cy5-siSNCA, blue; curcumin, green; and Dil-labeled exosome, red. (**F**) Western blot band of TSG101 and CD9 of EXO and REXO-C/ANP/S.

acquisition of REXO. The core C/ANP/S was obtained by a two-step process. First, we synthesized the polymers BA-poly(2-(dimethylamino)ethyl acrylate) (BAP) and BB-poly(2-(dimethylamino) ethyl acrylate) (BBP) (fig. S1A). BBP was used as a non–ROS-responsive control (*30*). $^{1}$H nuclear magnetic resonance of BAP and BBP indicated their successful synthesis (fig. S1, B to D). The amphiphilic polymer BAP could self-assemble and encapsulate the hydrophobic drug curcumin to form curcumin/BAP NP (C/ANP). The loading rate of curcumin in NP was calculated by Multiskan Spectrum, and the value was 70%. Next, the final C/ANP/siSNCA (C/ANP/S) and C/BNP/siSNCA (C/BNP/S) nanocomplex was formed via electrostatic interaction (Fig. 1A). We used the gel retardation assay and found that the siSNCA was completely attached to C/ANP at N/P (nitrogen portion of polymer/phosphorus portion of siRNA)

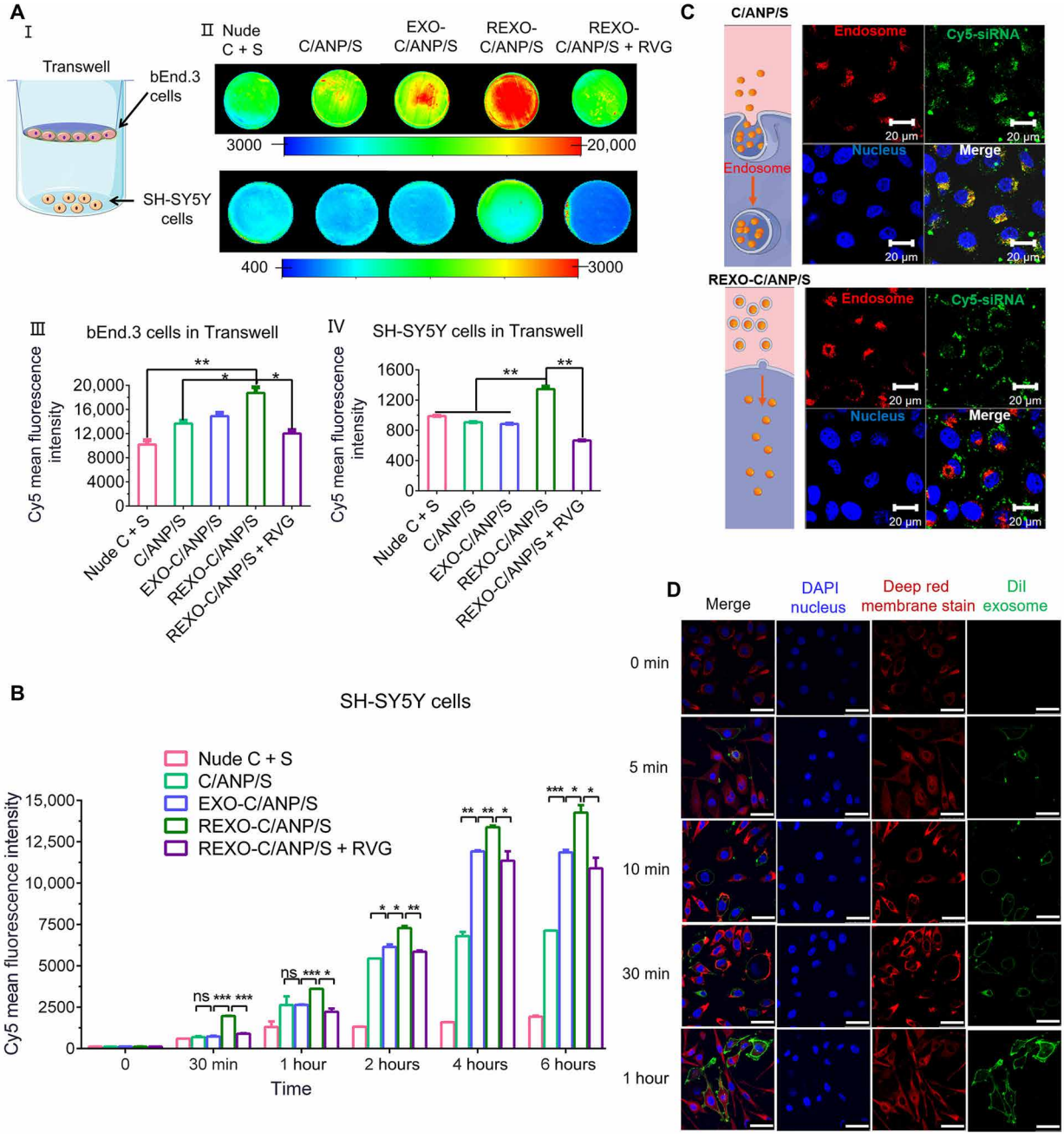


**Fig. 2. In vitro drug delivery.** (**A**) NP internalization in Transwell cells in 12 hours. I: Scheme of Transwell instrument. II: Cy5-siRNA internalization of bEnd.3 cells (top) and the SH-SH5Y cells (bottom). III: Cy5 mean fluorescence intensity in NP-treated bEnd.3 cells in Transwell model. IV: Cy5 mean fluorescence intensity in NP-treated SH-SH5Y cells in the Transwell model. (**B**) Cy5 mean fluorescence intensity detected by flow cytometry in SH-SH5Y cells after NP incubation in 0 min, 30 min, 1 hour, 2 hours, 4 hours, and 6 hours. ns, not significant. (**C**) Assessment by CLSM of SH-SY5Y cells after NP incubation in 4 hours. Endosome was labeled with LysoTracker red. Cy5-siSNCA, green. (**D**) Assessment by CLSM of SH-SY5Y cells after NP incubation in 0 min, 5 min, 10 min, 30 min, and 1 hour. Cell membrane was labeled with CellMask deep red membrane stain, and exosome was labeled with Dil.*$P < 0.05$, **$P < 0.01$, and ***$P < 0.001$. DAPI, 4′,6-diamidino-2-phenylindole.

of 5 (fig. S2A). The non–ROS-responsive C/BNP/S nanocomplex was prepared the same way, and it could also completely absorb siSNCA at an N/P ratio of 5 (fig. S2B). The morphology of C/ANP/S was a spherical shape of approximately 30 nm in diameter (fig. S2C). Furthermore, we simulated the cytoplasmic high ROS microenvironment of the diseased dopaminergic neuron in vitro and detected the ROS-responsive characteristics of both nanocomplexes (*31*). The non–ROS-responsive C/BNP/S slowly released curcumin in the phosphate-buffered saline (PBS) and $H_2O_2$ environment, and the final release ratios were 16.5 and 17.5% at 390 min, respectively (fig. S2D). The C/ANP/S had a low release rate of 24.4% in the PBS environment, but curcumin was more easily released in the $H_2O_2$ environment at a rate of 96.7% at 390 min. Therefore, C/ANP/S had the ROS-responsive drug release ability based on the material's structure.

The second part was the preparation of RVG-modified exosome REXO (Fig. 1A). First, bone marrow cells were extracted from the bone marrow of mice and were induced to differentiate into imDCs in vitro (*32*). The cell culture medium on the seventh day of culture was then collected. The cells and cell debris were removed by centrifugation. Next, culture medium was concentrated by ultrafiltration and passed through a qEV size exclusion column (Izon Science). The specified number 7, 8, and 9 fractions containing exosomes were separated and collected. Transmission electron microscopy (TEM) was used to identify the imDC exosome as a vesicle structure, approximately 70 nm in hydrodynamic diameter and with zeta potential of −12.7 mV (Fig. 2E). Targeted exosome could be engineered by click chemistry (*33*), targeting peptide plasmid transfer, or membrane fusion (*13*, *34*, *35*). However, these methods are complicated and time-consuming. In this engineering method, stearoyl-RVG was used to embed in the interior of the exosome phospholipid bilayer (table S1) (*36*). The mass spectrum confirmed the successful synthesis of the stearoyl-RVG (fig. S3A). To make the stearoyl-RVG visual in NPs, we then labeled it with fluorescein isothiocyanate (FITC). Stearoyl-RVG-FITC was synthesized by the condensation of amino group in stearoyl-$NH_2$ and carboxyl group in FITC-RVG (fig. S3B). After removing the unembedded stearoyl-RVG-FITC via ultrafiltration centrifugation, stearoyl-RVG-FITC was obtained. Stearoyl-RVG-FITC had a low solubility in PBS. Therefore, the improved fluorescence intensity of stearoyl-RVG-FITC in exosomes after the ultrasound method indicated its successful modification (fig. S3, C and D) (*36*). We further used the lipophilic dye DiD (red), which is a lipophilic tracer like DiR, to label exosomes (*37*). The colocalization coefficient of DiD exosomes and stearoyl-RVG-FITC was 0.95 (fig. S3E), indicating the successful modification of RVG on exosomes.

The assembly of the inner core and the outer REXO was carried out by the ultrasonic method using a bath sonicator at a frequency

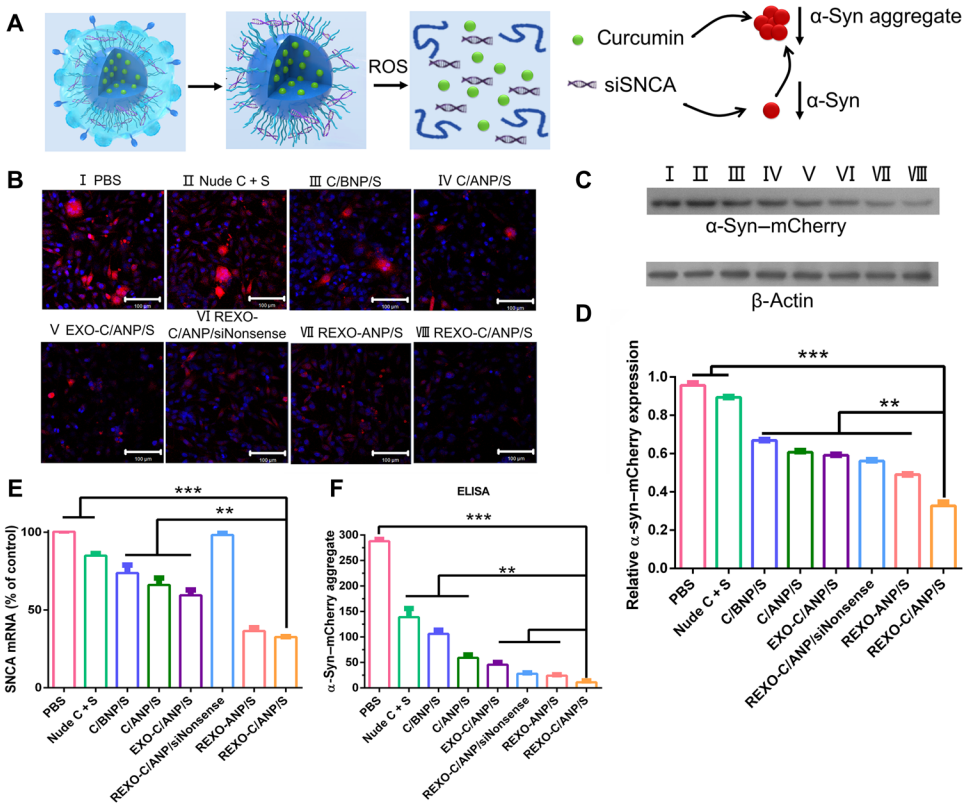


**Fig. 3. Effective pathological inhibition.** (**A**) Scheme of REXO-C/ANP/S synergistic effect against α-syn. (**B**) Effect of NPs on decrease in α-syn aggregates after NPs were incubated with SNCA–mCherry–SH-SY5Y cells. Scale bars, 100 μm. (**C**) Mouse α-syn–mCherry (anti–α-syn antibody) protein levels relative to β-actin by Western blot. Western blot band of cells incubated with different NPs. I, PBS; II, nude C + S; III, C/BNP/S; IV, C/ANP/S; V, EXO-C/ANP/S; VI, REXO-C/ANP/siNonsense; VII, REXO-ANP/S; and VIII, REXO-C/ANP/S. (**D**) Total α-syn protein levels were quantified relative to β-actin. (**E**) Total SNCA mRNA expression levels were quantified by quantitative reverse transcription polymerase chain reaction. (**F**) Total α-syn aggregate expression levels were quantified by ELISA. In (B) to (D) and (F), NPs were incubated with cells for 72 hours. In (E), NPs were incubated with cells for 36 hours. $^{**}P < 0.01$ and $^{***}P < 0.001$.

of 40 kHz and a power of 100 W (Fig. 1A) (*38*). The assembly process was assumed to be as shown in Fig. 1B and verified by TEM, size, and zeta potential measurement (Fig. 1C). Among the REXO and C/ANP/S complexes, below the REXO-to-C/ANP/S mass ratio of 0.05, the REXO absorbed to the surface of part C/ANP/S (Fig. 1C, I). The size of NPs increased to 141.0 nm at a mass ratio of 0.01, and the zeta potential decreased to 7.05 mV. At the ratio of 0.05, there was an intermediate state. The size increased to 437.5 nm, and TEM showed that C/ANP/S was cross-linked by the REXO (Fig. 1C, II). The ratio was further increased and, lastly, negative charge dominated the NPs that tended to be stable. The final core-shell monodisperse assembly forms as shown in Fig. 1C (III) at a mass ratio of 0.1, indicating that the REXO was coated on the surface of the core nanocomplexes. The final NP REXO-C/ANP/S was negatively charged at −7.1 mV, and the hydrodynamic diameter was 118.1 nm (Fig. 1D). Next, to facilitate the visual observation of the assembly components, we prepared positively charged poly-chitosan microspheres, which allowed adsorption of negatively charged assemblies on the surface (Fig. 1E). The exosomes were labeled with the lipophilic dye DiI. The result clearly showed the colocalization of DiI exosome, Cy5-siRNA, and curcumin (Fig. 1E and fig. S3F). In addition, the REXO-C/ANP/S obtained after assembly had the protein TSG101 and CD9 of EXO (Fig. 1F), which further indicated the successful coating.

## Enhanced drug delivery of REXO-C/ANP/S via REXO coating

In vitro, we investigated the biocompatibility of core nanocomplex C/ANP/S and the core-shell REXO-C/ANP/S. C/ANP/S and REXO-C/ANP/S were cocultured with SH-SY5Y cells under different N/P ratio conditions. As examined by 3-(4,5-dimethylthiazol-2-yl)-2,5-diphenyltetrazolium bromide (MTT) assay, the result showed that

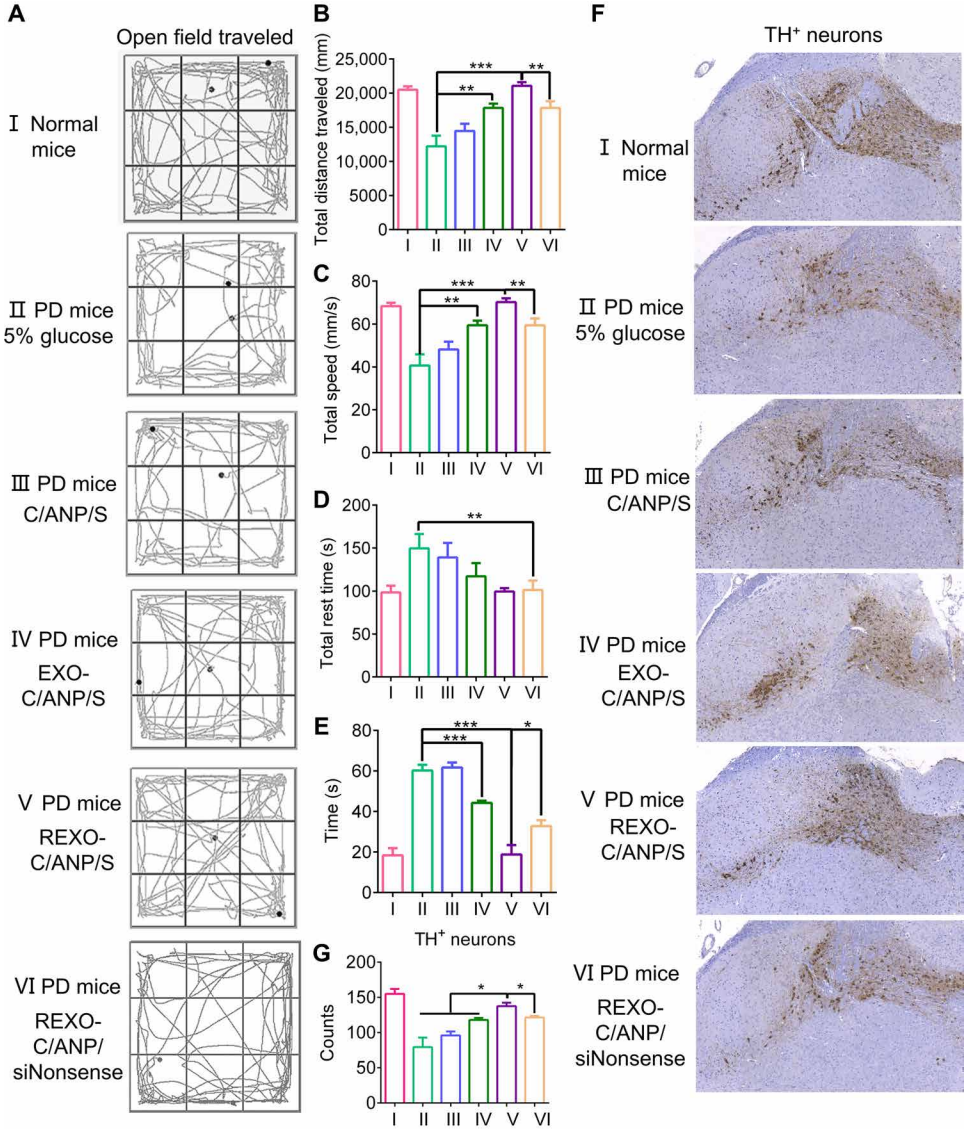


**Fig. 4. Enhanced neuronal recovery in vivo.** (**A**) Open-field traveled trace of normal mice and different NP-treated PD mice. (**B**) Total distance traveled of normal mice and different NP-treated PD mice in open field instrument. (**C**) Total speed of normal mice and different NP-treated PD mice in open field instrument. (**D**) Total rest time of normal mice and different NP-treated PD mice in open field instrument. (**E**) Time it took the mice to climb to the top in pole test. (**F**) TH immunohistochemistry staining (anti-TH antibody) of the brain slides in treated mice SN region. (**G**) Numbers of $TH^+$ neurons in the treated mice brain SN region. $^*P < 0.05$, $^{**}P < 0.01$, and $^{***}P < 0.001$.

the cell viability of both groups was above 80%. The survival rate under the experimental condition N/P ratio of 5/1 was 93.9% (fig. S4A), which was suitable for in vivo application.

Next, the delivery process was simulated in vitro to explore drug delivery of REXO-C/ANP/S and C/ANP/S. First, we used the Transwell culture method to simulate the BBB (Fig. 2A, I). bEnd.3 cells were cultured in Transwell inserts ($1 \times 10^5$ cells per polyester Transwell insert in six wells, pore diameter of 0.4 μm, 4.67 $cm^2$) for 7 days to a resulting monolayer with a transepithelial electrical resistance at least 200 ohm·$cm^2$. After adding NPs, Cy5 mean intensity fluorescence was detected by bioluminescence imaging using Kodak In-Vivo Imaging System FX Pro. The REXO coating significantly enhanced the uptake of siRNA drugs in C/ANP/S into bEnd.3 cells and then through the epithelial cells into lower SH-SY5Y cells (Fig. 2A, II to IV). As a comparison, the addition of free RVG peptide inhibited the promoting effect (Fig. 2A, II to IV). By comparing the uptake of siRNA in SH-SY5Y cells at different time points (Fig. 2B), it was found that the REXO coating significantly enhanced the uptake of the drugs in C/ANP/S. After 2 hours, the EXO and REXO coating groups EXO-C/ANP/S and REXO-C/ANP/S were significantly better than nude curcumin and siRNA (nude C + S) as well as the inner core C/ANP/S. This was because the C/ANP/S was

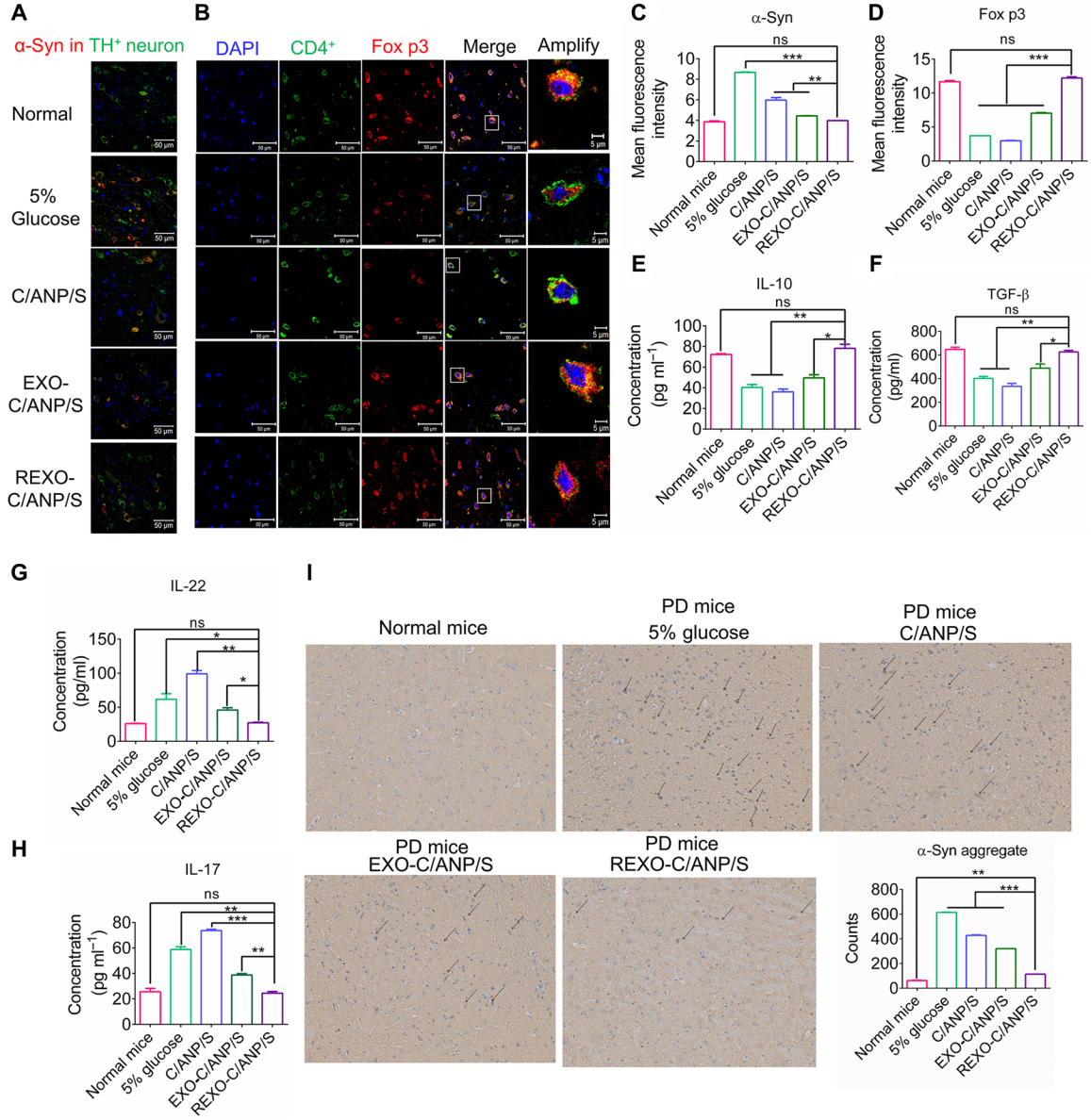


**Fig. 5. Nanoscavenging for PD mice.** (**A**) Immunofluorescence staining (anti-TH antibody and anti–α-syn antibody) of normal mice and different NP-treated PD mice. Scale bars, 50 μm. (**B**) Immunofluorescence staining (anti-CD4 antibody and anti–Fox p3 antibody) of normal mice and different NP-treated PD mice. Scale bars, 50 μm. The amplify images were the images in the white square, with a 5-μm scale bar. (**C**) α-Syn mean fluorescence intensity in (A). (**D**) Fox p3 mean fluorescence intensity in (B). (**E**) IL-10 concentration in serum of PD mice treated with NPs. (**F**) TGF-β concentration in serum of PD mice treated with NPs. (**G**) IL-22 concentration in serum of PD mice treated with NPs. (**H**) IL-17 concentration in serum of PD mice treated with NPs. (**I**) Conformation-specific α-syn aggregate immunohistochemistry staining (anti-conformation–specific MJFR α-syn aggregate antibody) of the brain slides in treated mice SN region. *$P < 0.05$, **$P < 0.01$, and ***$P < 0.001$.

endocytosed through the endosome-lysosome pathway due to quaternary amine compounds in the C/ANP/S, causing NP efflux and drug loss, so that the increased accumulation of drugs was not obvious with time (Fig. 2B) (*39*). The EXO-C/ANP/S and REXO-C/ANP/S avoided drug loss in the endosomal pathway after 2 hours, thereby enhancing drug accumulation. Second, the targeted RVG modification NP REXO-C/ANP/S more significantly increased the drug uptake than EXO-C/ANP/S. After the addition of the free RVG polypeptide, it inhibited the endocytosis of the drug due to its binding to the receptor on the cell surface, and the drug uptake was significantly reduced in the experimental results. Therefore, the results demonstrated that the exosome coating changed the endocytosis pathway, which has an important role in the increase of drug uptake.

Furthermore, to confirm the reason for the conjecture that the exosome coating C/ANP/S could avoid the drug loss of the endosome-lysosome pathway, we conducted an experiment to confirm whether the exogenous membrane fusion characteristics help. The results of the confocal laser scanning microscopy (CLSM) experiments showed a comparison of the endocytic mechanisms of the two systems (Fig. 2C). The core C/ANP/S was taken up through the endosome-lysosome pathway; thus, the drug aggregated in the endosomes (the overlap coefficient was 0.92 at 4 hours). However, the drug delivered by REXO-C/ANP/S was more dispersed in the cytoplasm, and therefore, there was less drug accumulation in the endosomes than C/ANP/S-treated cells (the overlap coefficient was 0.56 at 4 hours). Next, we labeled the exosomes with DiI and labeled the cell membrane with CellMask deep red membrane stain to detect the fusion of the two dyes in a short period. The fluorescence of DiI was enhanced with the extension of time, and it was apparently colocalized with the fluorescence of deep red membrane stain from 5 min to 1 hour (Fig. 2D and fig. S4B). These results demonstrated that the drug of REXO-C/ANP/S was enriched mostly through membrane fusion.

### Enhanced α-syn clearance by REXO-C/ANP/S

α-Syn aggregates were the main pathological substance in PD neurons. Therefore, it was very important to clear the α-syn aggregates and excess α-syn for PD treatment (Fig. 3A). We constructed an SH-SY5Y cell line SNCA–mCherry–SH-SY5Y cell, which overexpressed SNCA-mCherry protein by plasmid transfection and cell selection. First, we examined the effects of exosomes and RVG-modified exosomes on the α-syn expression and aggregates and found that there was almost no effect (fig. S4C). Next, nude drugs and different NPs were cocultured with SNCA–mCherry–SH-SY5Y cells for 2 days. The α-syn aggregates in α-syn–mCherry–overexpressing cell lines were observed by CLSM, in which mCherry was a red reporter for α-syn (Fig. 3B). The results of the total α-syn were also verified by Western blot [Fig. 3, C and D; 47 kDa (α-syn was 18 kDa, and mCherry was 29 kDa)]. There was a significant decrease in α-syn protein in the REXO-C/ANP/S–treated cells, compared with the blank (PBS) and the nude drug curcumin and siSNCA (nude C + S) groups. Compared with C/ANP/S, NPs without ROS-responsive C/BNP/S, and nontargeted EXO-C/ANP/S, the REXO-C/ANP/S had a stronger down-regulation effect, indicating the superiority of membrane fusion, target, and controlled-release ability. In addition, REXO-C/ANP/S had a down-regulation advantage compared with the curcumin-free NP REXO-ANP/S and the siNonsense NP REXO-C/ANP/siNonsense. In addition, except the REXO-C/ANP/siNonsense–treated cells, the SNCA mRNA expression of NP-treated cells was lower than PBS-treated cells. The SNCA mRNA expression of REXO-C/ANP/S–treated cells decreased 64% (Fig. 3E). Moreover, the enzyme-linked immunosorbent assay (ELISA) test showed that the α-syn aggregates in the cells treated by the drug-loaded NP groups were significantly reduced (Fig. 3F). In particular, α-syn aggregates in cells treated with gene-chem dual drug carrier REXO-C/ANP/S decreased most obviously. This was because the gene drug siSNCA avoided the development of excessive α-syn aggregation by reducing the synthesis of α-syn, and curcumin could directly inhibit α-syn aggregates. This result was consistent with our prediction. The gene-chem dual drug carrier relieves the pressure on neurons caused by the α-syn aggregate through the synergistic effect of two drugs. In addition, through dot blot experiments, similar results further showed that the gene-chem dual drug carrier reduced phosphorylated α-syn, conformation-specific α-syn aggregates, and oligomer A11 molecules, which were related molecularly to the formation of α-syn aggregates (fig. S4D). Obviously, it was proven that synergistic REXO-C/ANP/S had a delivery advantage at the cell level, and these contributed to substantially effective α-syn aggregate clearance. Furthermore, the changes in cellular ROS activity of nanomedicine-treated cells indicated their roles in anti-inflammation. The ROS level was evaluated in SNCA–mCherry–SH-SY5Y cells, and the intracellular ROS content was tested by CLSM. Treating the cells with curcumin-containing nanomedicine caused 2.7 times of ROS decrease (fig. S5) compared with treatment with PBS. However, the nanocarrier without curcumin REXO-ANP/S had little contribution to ROS decrease. Therefore, the results indicated that the curcumin loading in REXO-C/ANP/S had a strong role in inflammation regulation, but siSNCA alone had a weaker effect on ROS level than others in a short period of 72 hours.

### Enhanced neuronal recovery in vivo

In vivo, the enrichment of NPs in tissues is a key visualization tool for drug delivery. We detected drug distribution by using Kodak In-Vivo Imaging System FX Pro. Since curcumin itself has fluorescence property (excitation, 425 nm; emission, 530 nm), drug enrichment in the brain can be visualized in that the RVG29 peptide enhanced its accumulation in the brain (fig. S6, A and B). The accumulation of drug in the brain could last at least 48 hours (fig. S6, C and D). The drug was colocalized with tyrosine hydroxylase–positive ($TH^+$) neurons in the substantia nigra (SN) region in mice brain (fig. S6E), which was essential for treatment. 1-Methyl-4-phenyl-1,2,3,6-tetrahydropyridine (MPTP)–induced mice model of PD were vein injected with REXO-C/ANP/S and other control NPs (1 mg/kg siSNCA) every other day. After 10 times of administration, behavioral measurements were recorded. PD mice showed bradykinesia in the open field, and they traversed less in the middle region (Fig. 4A, II). Quantitative data in the open field for 30 min showed that their total distance decreased, movement speed slowed, and the rest time required was getting longer [Fig. 4, B to D (II)]. Mice in the NP groups showed a trend of improvement in exercise, especially the REXO-C/ANP/S group [Fig. 4, B to D (III to VI)]. In the pole experiment, the time to the tip of the rod was significantly reduced after the REXO-C/ANP/S treatment (Fig. 4E). This advantage was also shown in the brain sections after mouse dissection. Neuronal repair in the PD mice injected with REXO-C/ANP/S was better than in other groups (Fig. 4, F and G). In addition, hematoxylin-eosin staining of NP-treated mice organ slides indicated their safety without burden on the mice liver or other organs (fig. S7).

### Nanoscavenging of α-syn and aberrant immune activation

Furthermore, to explore the reasons for the superiority of the drug carrier REXO-C/ANP/S in neuroprotection, we discuss it from two aspects. First, the pathological substance α-syn in the neurons was a key substance that was needed to be cleared. By staining the SN region of treated mice, we concluded that the synergistic drug-loading C/ANP/S nanocomplex played a role in the clearance of α-syn in $TH^+$ neurons, but the scavenging effects of EXO-C/ANP/S and REXO-C/ANP/S were more pronounced, especially the targeted NP REXO-C/ANP/S (Fig. 5, A and C). This is due to the superior delivery advantages of targeted exosomes. In addition, we also explored improvements in the mouse immune microenvironment. The results indicated that T cell activation in mice with PD could be cleared by the action of the imDC exosomes coating themselves. After the mice were treated with NPs, we found that EXO-C/ANP/S, especially REXO-C/ANP/S, could significantly increase the expression of Fox p3 in CD4-positive ($CD4^+$) T cells (Fig. 5, B and D). In addition, REXO-C/ANP/S could significantly increase TGF-β and IL-10 in PD (Fig. 5, E and F). It has been proven that TGF-β signaling exerts anti-inflammatory effects, mainly neuroprotective effects. In addition, IL-22 and IL-17 were related to autoimmune diseases and were highly expressed as immune cytokines. Activated $T_H17$ cells secrete and produce IL-22 and IL-17 immune cytokines. As a result, REXO-C/ANP/S could significantly decrease the IL-22 and IL-17 factors in PD (Fig. 5, G and H). The results indicated that the exosomes from imDC could inhibit the immune activation of PD and that the target modification further enhanced their effect. In comparison, C/ANP/S had almost no effect on the immune regulation but instead activated the immune system. The results indicated that the exosomes from imDC could inhibit the immune activation of PD and that the target modification further enhanced their effect. Moreover, by staining the SN region of treated mice with phospho S129 α-syn antibody or polymerized α-syn MJFR-14-6-4-2 antibody from Abcam, we detected in pathological α-syn that the scavenging effects of EXO-C/ANP/S and REXO-C/ANP/S were more pronounced on phosphorylated α-syn and aggregated α-syn, especially the targeted NP REXO-C/ANP/S (Fig. 5I and fig. S8).

## DISCUSSION

In summary, combining the natural delivery advantages of exosomes with synthesized gene-chem nanocomplex, we designed a REXO coating gene-chem nanocomplex with high enrichment of drugs in the action site of a target cell. The role of REXO-C/ANP/S across the BBB and membrane fusion functions in α-syn aggregate clearance was confirmed at the cellular and animal levels. Efficient delivery of siRNA and chemical drugs by the target exosomes reduced the α-syn aggregates in diseased dopaminergic neurons (Fig. 6).

In addition, because of the natural immunomodulatory properties of the imDC exosomes, we discussed its role in clearing immune activation, which may be caused by α-syn peptides (*20*). $T_H17$ cells and $T_{reg}$ cells are $CD4^+$ T cell subsets. It has been reported that $T_H17$ cells have a strong inflammatory effect and play an important role in chronic inflammation and autoimmune diseases. $T_{reg}$ cells have obvious immunosuppressive effects and play an important role in immune tolerance and immune homeostasis. This delivery system can provide a functionalized vector for immunotherapy of neurodegenerative diseases (Fig. 6). This functionalization and exosome derived from imDC cells are inherited by major histocompatibility complex class II (MHC II), CD80, CD86, and other costimulatory

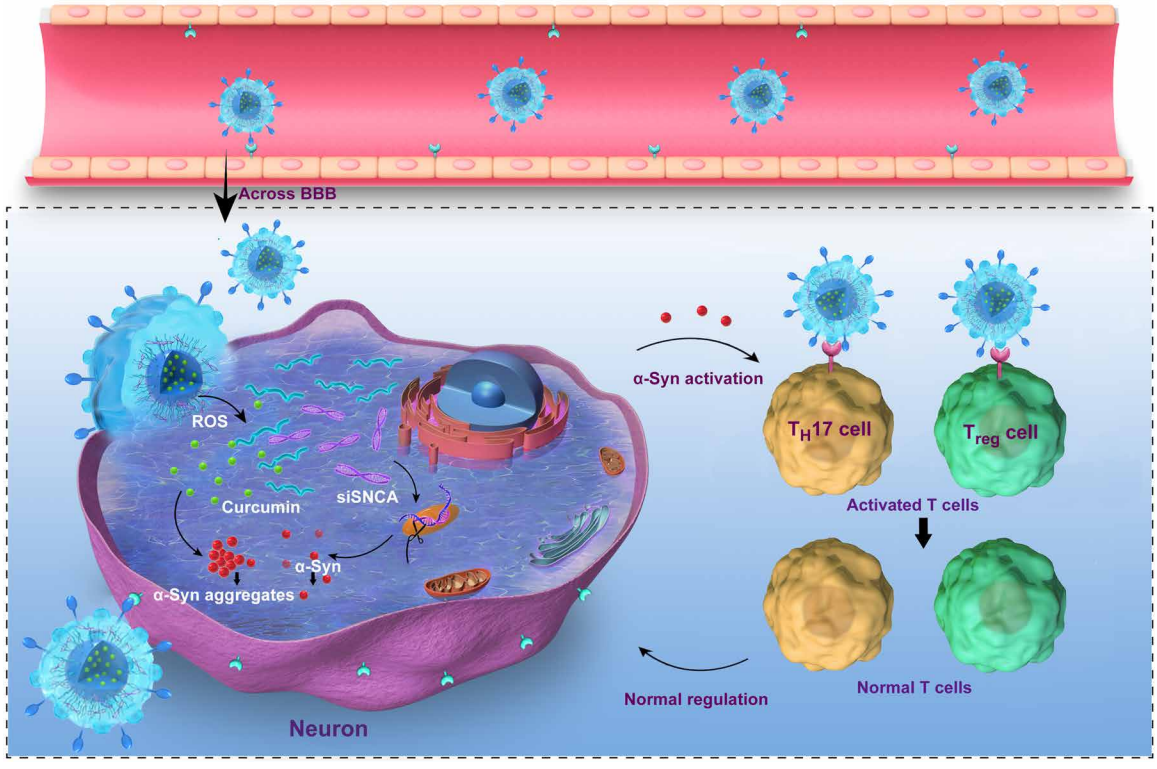


**Fig. 6. The potential mechanism of nanoscavenging.**

factors on the surface of imDC cells so that they also have immunosuppressive functions. Thus, regulation of $T_H17$ and $T_{reg}$ cell balance, which is inhibition of $T_H17$ differentiation and promotion of $T_{reg}$ production to induce immune tolerance, and reconstruction of immune homeostasis in vivo may be a therapeutic approach to neuronal protection in addition to the accumulation of misfolded proteins. Certain pathological substances, such as amyloid-β protein of Alzheimer's disease, are mostly the pathogenic cause of neurodegenerative diseases. Therefore, it can provide an efficient strategy for the treatment of neurodegenerative diseases.

## MATERIALS AND METHODS

### Chemicals and reagents

Curcumin was acquired from Melonepharma (Dalian, China), and siSNCA (table S1), Cy5-siSNCA, and negative control siSNCA (si-Nonsense, antisense strand, 5′-GACAAAUGUUGGAGGAGCATT-3′) were synthesized by GenePharma Company (Suzhou, China). RVG peptide was purchased from GL Biochem Ltd. Co. (Shanghai, China). Other chemicals in synthesis were from J&K Scientific Ltd. MTT and MPTP were obtained from Sigma-Aldrich. SH-SY5Y cells and SNCA–mCherry–SH-SY5Y cell line culture were the same as in the previous work (*11*).

### C/ANP/S core preparation

BAP and BBP were synthesized according to the method reported in our laboratory (*30*). The polymer BAP and BBP were dissolved in 100 μl of methanol to a concentration of 20 mg/ml, and curcumin was also dissolved in 100 μl of methanol to a concentration of 4 mg/ml. After mixing the two, the mixture was added dropwise to 2 ml of water or 5% glucose solution. After 3000-Da dialysis for 12 hours, the micelles C/ANP and C/BNP were obtained. C/ANP or C/BNP was incubated with siSNCA for 30 min at the appropriate N/P to obtain C/ANP/S or C/BNP/S. The incubation results were analyzed by gel electrophoresis. The final used N/P ratio was 5/1.

### Isolation and extraction of exosome

In general, exosomes were obtained from the primary bone marrow–derived imDC. Experimental animals were 6- to 8-week-old mice (C57BL/6), specific pathogen–free (SPF) grade, and from Weitonglihua Company (China). The femur and tibia were obtained from the euthanized mice, and the bone marrow was washed with RPMI 1640 medium. The red blood cells were lysed, and the remaining cells were suspended with complete medium [95% RPMI 1640 medium, 5% exosome-free fetal bovine serum, recombinant mouse granulocyte-macrophage colony-stimulating factor (rmGM-CSF; 20 ng/ml), and IL-4 (20 ng/ml)]. The cells were cultured at 37°C in an 5% $CO_2$ incubator, and the complete medium was changed half per 2 days. The cell culture medium on the seventh day was collected. Next, the collected medium was configured at 400*g* at 4°C for 5 min, the cells were removed, and the first supernatant was aspirated. Then, the supernatant was configured at 10,000*g* at 4°C for 60 min, cell debris were removed, and the second supernatant was obtained. Next, the second supernatant was centrifuged in a 100-kDa ultrafiltration tube at 5000*g* at 4°C for 30 min for three times, and 200 μl of the concentrated medium supernatant solution was obtained. Therefore, cells and cell debris were removed by centrifugation, and concentrated medium was obtained from ultrafiltration. At last, the exosome fraction was collected by a qEV size exclusion column (Izon Science) to remove the protein and big vesicles. The obtained exosomes were measured for protein concentration by the BCA (bicinchoninic acid assay) kit, and 125 μg of exosome was collected from one mouse. Exosomes were negatively stained with phosphotungstic acid–negative staining and observed under an electron microscope (JEM-1200EX).

### REXO-C/ANP/S preparation and characterization

RVG embedding exosome REXO was obtained by ultrasonic soaking for 5 min using an ultrasonic cleaner and cleaning three times by centrifugation through a 100-kDa ultrafiltration at 5000 revolutions per minute (rpm). REXO-C/ANP/S was prepared by ultrasonic soaking using a 40-kHz and 100-W ultrasonic cleaner for 15 min and cleaning three times by centrifugation through a 100-kDa ultrafiltration at 5000 rpm. Zeta potential and particle size of NPs were obtained by the Zetasizer Nano ZS90 (Malvern). The final mass ratio of C/ANP:siRNA:exosome was 4:1:0.5. NPs were observed under an electron microscope (JEM-1200EX).

### Chitosan microspheres

Chitosan (10,000 to 20,000 molecular weight) was dissolved in 0.9 weight % NaCl HAc-NaAc buffer solution and was adjusted to pH 4.5. Two milliliters of chitosan solution was poured into a 60-ml oil phase (a mixture with liquid paraffin–to–petroleum ether ratio of 7:5), containing 1.8 g of Span 80, with 4000 rpm homogenization for 5 min, and then was washed with petroleum ether for three times. The natural drying chitosan microsphere initial emulsion was obtained. For chitosan microsphere adsorption, 60 μl REXO-C/ANP/S was coincubated with 100 μl of the chitosan microspheres obtained above, and then slides were prepared and observed under a confocal microscope (Zeiss LSM780).

### Western blots

Briefly, exosome and cells were lysed in reducing sample buffer [8% SDS, 0.25 M tris-HCl (pH 6.8), 40% glycerol, 5% 2-mercaptoethanol, and 0.04% bromophenol blue] and boiled for 10 min at 95°C. Proteins were resolved by SDS–polyacrylamide gel electrophoresis, transferred to polyvinylidene fluoride membranes, blocked in 5% nonfat powdered milk in PBS-T (0.5% Tween 20), and probed with antibodies. They were incubated with antibodies (Abcam) and detected by an x-ray film after incubation with enhanced chemiluminescence reagent.

### In vitro study

The NP-treated SH-SY5Y cells and SNCA–mCherry–SH-SY5Y cells were collected and analyzed by BD Calibur Flow cytometry (BD Co., USA). Cells were cultured in glass-bottom dishes (Cellvis), and the Cy5 mean fluorescence intensity and α-syn–mCherry were calculated to measure the siRNA uptake using CLSM (Zeiss Co., Germany). Labeled exosome was obtained by incubating with 5 μM of DiD for 30 min. The unincorporated dyes were removed using 300-kDa ultrafiltration centrifugation. DiI-labeled cell membrane was dissolved in the medium at a working concentration of 5 μM. After coculture with the cells for 30 min, the medium was aspirated and washed repeatedly three times with the medium.

### PD mice therapy

Experimental animals were 6- to 8-week-old mice (C57BL/6), SPF grade. MPTP was purchased from Sigma-Aldrich. The mice were

intraperitoneally injected with MPTP (30 mg/kg) for seven consecutive days. In the treatment plan, mice were administered via tail vein injection with five numbers in each treatment group, and the cycle was once every other day for 10 times. After one treatment cycle, 100 μl of blood was taken from the eyelids and collected. The total time of observation in the open field experiment was 30 min. Mouse IL-17A ELISA kit and mouse IL-10 ELISA kit were from LAIZEE, China. After the mice were euthanized, the brain was removed, paraffin sections were prepared, and the brain sections of the SN were stained with anti–α-syn, anti-TH, anti–Fox p3, and anti-CD4 antibody (Abcam). Presence of α-syn aggregates in $TH^+$ neurons and the presence of Fox p3 were analyzed by immune fluorescence staining. $TH^+$ neurons were analyzed by immunohistochemistry staining. All procedures involving experimental animals were performed in accordance with protocols approved by the Institutional Animal Care and Use Committee of Peking University.

## SUPPLEMENTARY MATERIALS

Supplementary material for this article is available at http://advances.sciencemag.org/cgi/content/full/6/50/eaba3967/DC1

View/request a protocol for this paper from *Bio-protocol*.

## REFERENCES AND NOTES


1. S. B. Dunnett, A. Björklund, Prospects for new restorative and neuroprotective treatments in Parkinson's disease. *Nature* **399**, A32–A39 (1999).
2. M. G. Spillantini, M. L. Schmidt, V. M.-Y. Lee, J. Q. Trojanowski, R. Jakes, M. Goedert, α-Synuclein in Lewy bodies. *Nature* **388**, 839–840 (1997).
3. S. Makin, Pathology: The prion principle. *Nature* **538**, S13–S16 (2016).
4. J. M. Cooper, P. B. O. Wiklander, J. Z. Nordin, R. Al-Shawi, M. J. Wood, M. Vithlani, A. H. V. Schapira, J. P. Simons, S. El-Andaloussi, L. Alvarez-Erviti, Systemic exosomal siRNA delivery reduced alpha-synuclein aggregates in brains of transgenic mice. *Mov. Disord.* **29**, 1476–1485 (2014).
5. N. Sharma, B. Nehru, Curcumin affords neuroprotection and inhibits α-synuclein aggregation in lipopolysaccharide-induced Parkinson's disease model. *Inflammopharmacology* **26**, 349–360 (2017).
6. P. K. Singh, V. Kotia, D. Ghosh, G. M. Mohite, A. Kumar, S. K. Maji, Curcumin modulates α-synuclein aggregation and toxicity. *ACS Chem. Nerosci.* **4**, 393–407 (2013).
7. B. Ahmad, L. J. Lapidus, Curcumin prevents aggregation in α-synuclein by increasing reconfiguration rate. *J. Biol. Chem.* **287**, 9193–9199 (2012).
8. W. M. Pardridge, shRNA and siRNA delivery to the brain. *Adv. Drug Deliv. Rev.* **59**, 141–152 (2007).
9. P. Anand, A. B. Kunnumakkara, R. A. Newman, B. B. Aggarwal, Bioavailability of curcumin: Problems and promises. *Mol. Pharm.* **4**, 807–818 (2007).
10. C. Betsholtz, Physiology: Double function at the blood-brain barrier. *Nature* **509**, 432–423 (2014).
11. L. Liu, Y. Li, R. Liu, Q. Shen, Y. Li, Z. Shi, J. Shen, W. Ji, X. Zhang, Switchable nanoparticle for programmed gene-chem delivery with enhanced neuronal recovery and CT imaging for neurodegenerative disease treatment. *Mater. Horiz.* **6**, 1923–1929 (2019).
12. V. Hornung, F. Bauernfeind, A. Halle, E. O. Samstad, H. Kono, K. L. Rock, K. A. Fitzgerald, E. Latz, Silica crystals and aluminum salts activate the NALP3 inflammasome through phagosomal destabilization. *Nat. Immunol.* **9**, 847–856 (2008).
13. L. Alvarez-Erviti, Y. Seow, H. Yin, C. Betts, S. Lakhal, M. J. A. Wood, Delivery of siRNA to the mouse brain by systemic injection of targeted exosomes. *Nat. Biotechnol.* **29**, 341–345 (2011).
14. E. V. Batrakova, M. S. Kim, Using exosomes, naturally-equipped nanocarriers, for drug delivery. *J. Control. Release* **219**, 396–405 (2015).
15. J. G. van der Boorn, M. Schlee, C. Coch, G. Hartmann, SiRNA delivery with exosome nanoparticles. *Nat. Biotechnol.* **29**, 325–326 (2011).
16. Y. Tian, S. Li, J. Song, T. Ji, M. Zhu, G. J. Anderson, J. Wei, G. Nie, A doxorubicin delivery platform using engineered natural membrane vesicle exosomes for targeted tumor therapy. *Biomaterials* **35**, 2383–2390 (2014).
17. Y. Liu, R. Huang, L. Han, W. Ke, K. Shao, L. Ye, J. Lou, C. Jiang, Brain-targeting gene delivery and cellular internalization mechanisms for modified rabies virus glycoprotein RVG29 nanoparticles. *Biomaterials* **30**, 4195–4202 (2009).
18. T. Korn, A. Kallies, T cell responses in the central nervous system. *Nat. Rev. Immunol.* **17**, 179–194 (2017).
19. J. A. H. Saunders, K. A. Estes, L. M. Kosloski, H. E. Allen, K. M. Dempsey, D. R. Torres-Russotto, J. L. Meza, P. M. Santamaria, J. M. Bertoni, D. L. Murman, H. H. Ali, D. G. Standaert, R. L. Mosley, H. E. Gendelman, CD4+ regulatory and effector/memory T cell subsets profile motor dysfunction in Parkinson's disease. *J. Neuroimmune Pharmacol.* **7**, 927–938 (2012).
20. D. Sulzer, R. N. Alcalay, F. Garretti, L. Cote, E. Kanter, J. Agin-Liebes, C. Liong, C. M. Murtrey, W. H. Hildebrand, X. Mao, V. L. Dawson, T. M. Dawson, C. Oseroff, J. Pham, J. Sidney, M. B. Dillon, C. Carpenter, D. Weiskopf, E. Phillips, S. Mallal, B. Peters, A. Frazier, C. S. Lindestam Arlehamn, A. Sette, T cells from patients with Parkinson's disease recognize α-synuclein peptides. *Nature* **546**, 656–661 (2017).
21. A. Sommer, F. Marxreiter, F. Krach, T. Fadler, J. Grosch, M. Maroni, D. Graef, E. Eberhardt, M. J. Riemenschneider, G. W. Yeo, Z. Kohl, W. Xiang, F. H. Gage, J. Winkler, I. Prots, B. Winner, Th17 lymphocytes induce neuronal cell death in a human iPSC-based model of Parkinson's disease. *Cell Stem Cell* **24**, 1006 (2019).
22. H. Kebir, K. Kreymborg, I. Ifergan, A. Dodelet-Devillers, R. Cayrol, M. Bernard, F. Giuliani, N. Arbour, B. Becher, A. Prat, Human $T_H17$ lymphocytes promote blood-brain barrier disruption and central nervous system inflammation. *Nat. Med.* **13**, 1173–1175 (2007).
23. T. Korn, A. Kallies, Interleukin-10 protects against inflammation-mediated degeneration of dopaminergic neurons in substantia nigra. *Neurobiol. Aging* **28**, 894–906 (2007).
24. I. Kryczek, S. Wei, L. Zou, G. Zhu, P. Mottram, H. Xu, L. Chen, W. Zou, Cutting edge: Induction of B7–H4 on APCs through IL-10: Novel suppressive mode for regulatory T cells. *J. Immunol.* **177**, 40–44 (2006).
25. A. D. Reynolds, D. K. Stone, R. L. Mosley, H. E. Gendelman, Nitrated α-synuclein-induced alterations in microglial immunity are regulated by $CD4^+$ T cell subsets. *J. Immunol.* **182**, 4137–4149 (2009).
26. I. Zanoni, F. Granucci, The regulatory role of dendritic cells in the induction and maintenance of T-cell tolerance. *Autoimmunity* **4**, 23–32 (2011).
27. H. Yang, Y. Zhang, M. Wu, J. Li, W. Zhou, G. Li, X. Li, B. Xiao, P. Christadoss, Suppression of ongoing experimental autoimmune myasthenia gravis by transfer of RelB-silenced bone marrow dendritic cells is associated with a change from a T helper Th17/Th1 to a Th2 and $Foxp3^+$ regulatory T cell profile. *Inflamm. Res.* **59**, 197–205 (2010).
28. N. Cools, V. F. I. Van Tendeloo, E. L. J. M. Smits, M. Lenjou, G. Nijs, D. R. Van Bockstaele, Z. N. Berneman, P. Ponsaerts, Immunosuppression induced by immature dendritic cells is mediated by TGF-β/IL-10 double-positive $CD4^+$ regulatory T cells. *J. Cell. Mol. Med.* **12**, 690–700 (2008).
29. W. Yin, S. Ouyang, Y. Li, B. Xiao, H. Yang, Immature dendritic cell-derived exosomes: A promise subcellular vaccine for autoimmunity. *Inflammation* **36**, 232–240 (2013).
30. C. Qiao, J. Yang, Q. Shen, R. Liu, Y. Li, Y. Shi, J. Chen, Y. Shen, Z. Xiao, J. Weng, X. Zhang, Traceable nanoparticles with dual targeting and ROS response for RNAi-based immunochemotherapy of intracranial glioblastoma treatment. *Adv. Mater.* **30**, 1705054 (2018).
31. C.-U. Cheong, C.-S. Yeh, Y.-W. Hsieh, Y.-R. Lee, M.-Y. Lin, C.-Y. Chen, C.-H. Lee, Protective effects of costunolide against hydrogen peroxide-induced injury in PC12 cells. *Molecules* **21**, 898 (2016).
32. Y.-I. Son, S.-i. Egawa, T. Tatsumi, R. E. Redlinger Jr., P. Kalinski, T. Kanto, A novel bulk-culture method for generating mature dendritic cells from mouse bone marrow cells. *J. Immunol. Methods* **262**, 145–157 (2002).
33. T. Smyth, K. Petrova, N. M. Payton, I. Persaud, J. S. Redzic, M. W. Graner, P. Smith-Jones, T. J. Anchordoquy, Surface functionalization of exosomes using click chemistry. *Bioconjug. Chem.* **25**, 1777–1784 (2014).
34. Y. Liu, D. Li, Z. Liu, Y. Zhou, D. Chu, X. Li, X. Jiang, D. Hou, X. Chen, Y. Chen, Z. Yang, L. Jin, W. Jiang, C. Tian, G. Zhou, K. Zen, J. Zhang, Y. Zhang, J. Li, C.-Y. Zhang, Targeted exosome-mediated delivery of opioid receptor Mu siRNA for the treatment of morphine relapse. *Sci. Rep.* **5**, 17543 (2015).
35. Y. T. Sato, K. Umezaki, S. Sawada, S. A. Mukai, Y. Sasaki, N. Harada, H. Shiku, K. Akiyoshi, Engineering hybrid exosomes by membrane fusion with liposomes. *Sci. Rep.* **6**, 21933 (2016).
36. Q. Tian, C. He, G. Liu, Y. Zhao, L. Hui, Y. Mu, R. Tang, Y. Luo, S. Zheng, B. Wang, Nanoparticle counting by microscopic digital detection: Selective quantitative analysis of exosomes via surface-anchored nucleic acid amplification. *Anal. Chem.* **90**, 6556–6562 (2018).
37. O. P. B. Wiklander, J. Z. Nordin, A. O'Loughlin, Y. Gustafsson, G. Corso, I. Mäger, P. Vader, Y. Lee, H. Sork, Y. Seow, N. Heldring, L. Alvarez-Erviti, C. I. E. Smith, K. L. Blanc, P. Macchiarini, P. Jungebluth, M. J. A. Wood, S. E. Andaloussi, Extracellular vesicle in vivo biodistribution is determined by cell source, route of administration and targeting. *J. Extracell. Vesicles* **4**, 26316 (2015).
38. C.-M. J. Hu, R. H. Fang, K.-C. Wang, B. T. Luk, S. Thamphiwatana, D. Dehaini, P. Nguyen, P. Angsantikul, C. H. Wen, A. V. Kroll, C. Carpenter, M. Ramesh, V. Qu, S. H. Patel, J. Zhu, W. Shi, F. M. Hofman, T. C. Chen, W. Gao, K. Zhang, S. Chien, L. Zhang, Nanoparticle biointerfacing by platelet membrane cloaking. *Nature* **526**, 118–121 (2015).

39. C. S. Kim, N. D. B. Le, Y. Xing, B. Yan, G. Y. Tonga, C. Kim, R. W. Vachet, V. M. Rotello, The role of surface functionality in nanoparticle exocytosis. *Adv. Healthc. Mater.* **3**, 1200–1202 (2014).

**Acknowledgments**
**Funding:** This work was financially supported by the Beijing Nova Program (Z201100006820140), the National High Technology Research and Development Program (2016YFA0200303), the National Natural Science Foundation of China (21905283, 31771095, and 21875254), and the Beijing Natural Science Foundation (2192057 and L172046). **Author contributions:** L.L., Y.L., and X.Z. designed the experiments. L.L., Y.L., H.P., R.L., W.J., and J.S. performed the experiments. L.L., Y.L., and X.Z. wrote the manuscript. Z.S. and G.M. edited the manuscript. All the authors analyzed the data and contributed to the paper. **Competing interests:** The authors declare that they have no competing interests. **Data and materials availability:** All data needed to evaluate the conclusions in the paper are present in the paper and/or the Supplementary Materials. Additional data related to this paper may be requested from the authors.

Submitted 29 November 2019
Accepted 22 October 2020
Published 11 December 2020
10.1126/sciadv.aba3967

**Citation:** L. Liu, Y. Li, H. Peng, R. Liu, W. Ji, Z. Shi, J. Shen, G. Ma, X. Zhang, Targeted exosome coating gene-chem nanocomplex as "nanoscavenger" for clearing α-synuclein and immune activation of Parkinson's disease. *Sci. Adv.* **6**, eaba3967 (2020).